PREPARATION AND CHARACTERIZATION OF SEVERAL PYRIMIDINE DERIVATIVES AND EVALUATION OF THEIR ANTIBACTERIAL AND ANTICANCER ACTIVITY

Mona R. Hamdy*, Qader A. Shannak

Department of Chemistry, College of Education for Pure Sciences, Tikrit University, Tikrit, Iraq
**e-mail: mr230001pep@st.tu.edu.iq*

Received 17.03.2025
Accepted 21.05.2025

Abstract: *This study included the preparation of several hexagonal rings derived from pyrimidines. Alpha-beta-unsaturated compounds were prepared by reacting 4-methyl thiazole-5-carbaldehyde with acetophenone substitutes. This step was considered the nucleus for the preparation of hexagonal rings. Then, the alpha-beta-unsaturated compounds were treated with several reagents to obtain pyrimidine derivatives in equal molar ratios. They reacted with urea to form 2-oxopyrimidine and with thiourea to form 2-thiopyrimidine. In the final step, they were reacted with cyanoguanidine to form 2-cyanamide pyrimidine. The catalyst in all cases was sodium hydroxide, and the solvent was ethanol. Physical and spectroscopic techniques, including infrared and nuclear magnetic resonance spectroscopy of protons and carbons, were used to confirm the compounds' structures. Thin-layer chromatography (TLC) was used to monitor the reaction progress and determine melting points and purity. Two bacterial isolates, one Gram-positive (Staphylococcus aureus) and one Gram-negative (Escherichia coli), were used to study the effects of several of the produced chemicals on their growth. Several synthesized compounds had strong inhibitory efficacy against the examined microorganisms, while the antibiotic amoxicillin was a control. Furthermore, the prepared compounds (MC7, MC15, and MC19) were tested for their ability to inhibit the growth of human breast cancer cells (MCF-7) in vitro. These cells were treated with six concentrations (50, 100, 200, and 400) µg/ml. The results showed a dose-dependent cellular response, where the survival rate of cancer cells decreased with increasing concentration ($P \leq 0.0001$). In contrast, normal cells were affected to a lesser extent, indicating the possibility of the compounds' selectivity against cancer cells.*

Keywords: *Heterocycles, Chalcone, Pyrimidine, Cancer, Biological activity.*
DOI: 10.65382/2221-8688-2026-2-183-199

1. Introduction

A major worldwide health issue that affects many individuals is cancer. In 2020, there were around 10 million cancer-related deaths and 19.3 million new instances of cancer, making it the world's top cause of death [1]. Lung cancer accounted for 18% (1.8 million) of these cases, and colorectal, liver, stomach, and breast cancers in women accounted for 9.4%, 8.3%, 7.7%, and 6.9% of subsequent deaths, respectively. The number of new cancer cases worldwide is predicted to increase by 47% between 2020 and 2040, underscoring the need for innovative treatment agents to fight this illness [1].

Heterocycles provide an alluring chance to find new compounds for cancer treatment, particularly heterocyclic clusters. According to science, almost 85% of all molecules with biological activity are heterocyclic or made up of a heterocyclic ring. Complex structures of these compounds are frequently based on heterocyclic rings that include nitrogen. These specifics highlight the crucial role that heterocyclic rings play in drug design and ongoing discovery. The most prevalent of these substances are nitrogen-containing heterocyclic compounds, which are found in vitamins, hormones, and antibiotics [2]. The US Food and Drug Administration database indicates that nitrogen-containing heterocyclic rings make up 60% of exclusive medicines (small molecules), underscoring the structural significance of these chemicals in medication discovery and design [3, 4]. Because of their stability and functional effectiveness in human anatomy, as well as proof that nitrogen atoms

easily form hydrogen bonds with DNA, nitrogen heterocyclization is common in physiologically active chemicals. Nitrogen-based heterocyclic compounds' affinity for DNA through hydrogen bonding is largely responsible for their anticancer properties [5]. According to the majority of medications that have received FDA approval, they include a pyrimidine core with a variety of alterations. Additionally, in cancer research, pyridine and its derivatives show promise as anticancer drugs. Pyrimidine They are heterocyclic compounds similar to pyridine, consisting of two nitrogen atoms and four carbon atoms in the ring, and are in the form of 1,3-hexacyclic heterocyclic diazines. Pyrimidines are found in genetic materials and natural goods [6]. Carcinogenesis is one of the many biological processes that have been connected to pyrimidine substructures. The potential therapeutic effects of pyrimidines and their derivatives in a number of malignant diseases, including idiopathic respiratory fibrosis, myeloid leukemia, and breast cancer, have drawn much attention in recent medical research [6, 7]. Sorafenib is one of the authorized medications that contain pyrimidine molecules.

The current study aims to prepare a number of pyrimidine compounds and evaluate their anti-cancer and anti-bacterial activity.

2. Experimental part

2.1. Material. Fluka, Aldrich, and BDH supplied all of the compounds utilized in this investigation, and none of them required additional purification.

2.2. Devices used. Melting points were determined with a 9300 thermoelectric melting apparatus. Spectra were recorded on a Shimadzu FT-IR 8400S spectrometer at (400-4000) cm^{-1} using a KBr disc for bromine. ^{1}H-NMR and ^{13}C-NMR spectra were recorded on Bruker instruments operating at 400 MHz. TLC was performed using 0.2 mm thick Fluka silica gel plates activated with Fluorine G silica gel, and the plates were visualized using UV light. The media used in the study were sterilized with a steam sterilizer from RAIBBA (Spain) developed for the research laboratory at Tikrit University. The plates used in the microbiological study were incubated using a Heraeus D-63450 incubator (Germany) at the same facility.

2.3. Preparation of Chalcone derivatives (MC_1-MC_5)

Dissolve 0.01 mol (1.2 g) of 4-methylthiazole-5-carbaldehyde in 20 mL of ethanol. Add 5 mL of 20% alcoholic sodium hydroxide solution and stir for 10 minutes. Subsequently, add 0.01 mol of the substituted acetophenone to the reaction mixture and maintain the mixture at 20–40 °C for 3 hours [8, 9]. After completion, pour the reaction mixture onto crushed ice to induce precipitation. Keep the mixture in a refrigerator overnight. Filter the precipitate, and then recrystallize it from ethanol (see Table 1).

2.4. Preparation of pyrimidines derivatives (MC_6-MC_{20})

In a 100-mL round-bottom flask, 0.004 mol of the synthesized chalcone derivatives [MC1–MC5] were dissolved in 10 mL of absolute ethanol. To this solution, 0.004 mol of urea (0.24 g), thiourea (0.30 g), or cyanoguanidine (0.33 g), each dissolved in 10 mL of ethanol, was added. Subsequently, 10 mL of 10% aqueous sodium hydroxide solution was introduced to increase the alkalinity, thereby promoting the reaction between the chalcone and urea (or thiourea) [10, 11]. The reaction mixture was stirred continuously for 6 h.

After completion, the pH was adjusted to 7 by the dropwise addition of 10% hydrochloric acid solution. The mixture was cooled and poured onto crushed ice to induce precipitation. The solid product was collected by filtration, washed thoroughly with cold water, and recrystallized from methanol (see Table 1).

Table 1. Some physical properties of the prepared compounds (MC_1-MC_{20})

Comp No.	R	Molecular Formula/ M.Wt g/mol	Color	M.P (^{0}C)	Yield (%)
MC_1	Br	$C_{13}H_{10}BrNOS$ 308.19	Light yellow	91-93	78
MC_2	NO_2	$C_{13}H_{10}N_2O_3S$ 274.29	Brown	160-162	81
MC_3	OCH_3	$C_{14}H_{13}NO_2S$ 259.32	Light yellow	98-101	82

MC_4	H	$C_{13}H_{11}NOS$ 229.30	Light yellow	99-101	78
MC_5	Cl	$C_{13}H_{10}ClNOS$ 263.74	Orange	97-99	80
MC_6	Br	$C_{14}H_{12}BrN_3OS$ 350.23	Dark Brown	135-137	70
MC_7	NO_2	$C_{14}H_{12}N_4O_3S$ 316.34	Dark Red	190-193	65
MC_8	OCH_3	$C_{15}H_{15}N_3O_2S$ 301.36	Read	149-152	71
MC_9	H	$C_{14}H_{13}N_3OS$ 271.34	Dark Green	140-142	62
MC_{10}	Cl	$C_{14}H_{12}ClN_3OS$ 305.78	Dark yellow	150-152	64
MC_{11}	Br	$C_{14}H_{12}BrN_3S_2$ 366.30	Light Yellow	126-128	57
MC_{12}	NO_2	$C_{14}H_{12}N_4O_2S_2$ 332.40	Dark Brown	250-253	63
MC_{13}	OCH_3	$C_{15}H_{15}N_3OS_2$ 317.43	Light Yellow	183-185	64
MC_{14}	H	$C_{14}H_{13}N_3S_2$ 287.40	Orange	117-119	59
MC_{15}	Cl	$C_{14}H_{12}ClN_3S_2$ 321.84	Orange	211-213	60
MC_{16}	Br	$C_{15}H_{12}BrN_5S$ 374.26	Yellow	130-132	62
MC_{17}	NO_2	$C_{15}H_{12}N_6O_2S$ 340.36	Dark Brown	206-208	58
MC_{18}	OCH_3	$C_{16}H_{15}N_5OS$ 325.39	Dark Yellow	131-133	63
MC_{19}	H	$C_{15}H_{13}N_5S$ 295.36	Yellow	140-142	59
MC_{20}	Cl	$C_{15}H_{12}ClN_5S$ 329.81	Yellow	138-140	55

2.5. Biological activity study. This study employed two different forms of harmful bacteria: Gram-negative *Escherichia coli*, and Gram-positive *Staphylococcus aureus*. Because of their antibiotic resistance, these microorganisms are vital to the medical industry. These microorganisms were gathered from the Department of Life Sciences' labs at the College of Education for Pure Sciences. Mueller Hinton agar, a culture medium used to assess the biological activity of antibiotics and other compounds having therapeutic applications, was employed [12]. It is employed to quantify and ascertain the MIC, or minimal inhibitory concentration. (DMSO) solvent was used to create chemical solutions for a few of the compounds at concentrations of (0.1, 0.01, 0.001) mg/ml. The diffusion technique in a Mueller Hinton agar nutrient medium was employed to examine the susceptibility of the bacterial isolates utilized in the study [13]. Since increasing the inhibition diameter increases the biological activity of the prepared compounds, To demonstrate the sensitivity of the employed derivatives, the data were read the next day. This sensitivity is compared to the inhibition diameter of antibiotics and is reliant on the apparent inhibition diameter in the dishes around the holes utilized [14].

2.6. MTT Cytotoxicity Assay. In this study, the effects of the compounds (MC_7, MC_{15}, and MC_{19}) on HdFn model cells, as well as MCF-7 breast cancer cells, were evaluated at different concentrations (400, 200, 100, and 50 µg/ml). Initially, the cells involved in the study were cultured and placed in an incubator containing carbon dioxide at 37°C. Subsequently, the concentrations of the compounds that affected the cancer cells were reduced to several known concentrations (50, 100, 200, and 400 µg/ml). Subsequently, each dose of the prepared concentration of the compounds (MC_7, MC_{15}, MC_{19}) was added to the MCF-7 cells. These cultured cells were allowed to incubate for a sufficient period at 37°C in the presence of 5% carbon dioxide. Next, 10 µL of MTT suspension was added to the test tubes and incubated again at 37°C with 5% atmospheric carbon dioxide. The intermediate solutions were then discarded, and one solution was added to each test tube to dissolve the formazan crystals. After the complete incubation period in a humidified environment, the absorbance of the samples was recorded at 575 nm using a Bio-rad reader, an ELISA machine made in Germany, and statistical analysis was performed using a GraphPad Prism [15, 16].

3. Results and discussion

The Scheme 1 shows the series of preparations of pyrimidine derivatives by reacting urea with chalcone to produce 2-oxopyrimidine, reacting thiourea with chalcone to produce 2-thiopyrimidine, and reacting

cyanoguanidine with chalcone to form 2-pyrimidine cyanamide. These reactions occurred in equal molar ratios.

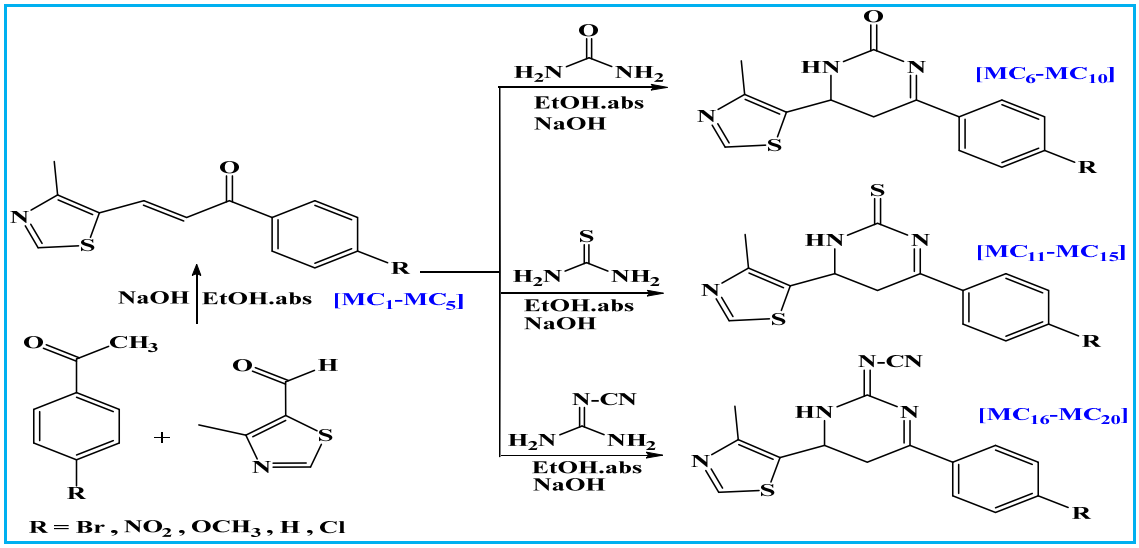

Scheme 1. Route of prepared compounds (MC_1-MC_{20})

3.1. Characterization of Chalcone derivatives (MC_1-MC_5). Studying of the infrared spectrum (FT-IR) showed that the stretching of the aromatic (CH) bond was responsible for the observation of an absorption band in the 3052-3072 cm^{-1} region. The carbonyl group and the double bond that emerged in the region 1600-1616 cm^{-1} alternated, which is why a rise in the wavenumber of the ketone carbonyl group (C=O) was also seen in the range 1663-1669 cm^{-1}. As a result, the double bond's wavenumber decreases due to a decrease in its force constant. Additionally, the spectrum displayed a signal in the 3139-3174 cm^{-1} range, which was caused by the olefin (=CH) bond stretching. In addition to the existence of two absorption bands in the 2920–2946 and 2825–2861 cm^{-1} ranges, which are ascribed to the aliphatic (CH) bond's symmetric and asymmetric stretching, respectively. Additionally, an absorption band that stretched the aromatic bond (C=C) was seen, extending in the ranges of (1581-1508 & 1481-1460) cm^{-1} [17, 18] (see Table 2 and Fig. 1).

Table 2. FT-IR absorption results for Chalcone derivatives (MC_1-MC_5)

Comp. No.	R	IR (KBr) cm^{-1}						
		ν(C-H) Arom.	ν(C-H) Aliph.	ν(C-H) Olph.	ν C=O	ν(C=C) Olph.	ν(C=C) Arom.	Others
MC_1	Br	3064	2920 2850	3153	1664	1600	1508 1460	ν (C-Br) 609
MC_2	NO_2	3072	2920 2850	3159	1663	1616	1581 1481	ν(NO_2) *asy*. (1531) *sym*. (1352)
MC_3	OCH_3	3052	2946 2825	3161	1667	1604	1570 1468	νC-O-C Asy: 1347 sym: 1264
MC_4	H	3061	2944 2861	3174	1665	1609	1566 1470	---
MC_5	Cl	3067	2938 2851	3139	1669	1612	1545 1462	ν (C-Cl)759

The ^{1}H-NMR spectrum of compound MC$_1$ was recorded in DMSO-d$_6$. A singlet at δ8.15 ppm was assigned to the proton of the N=CH group in the thiazole ring. Multiplet signals in the range δ7.27–7.71 ppm corresponded to the aromatic protons. A doublet at δ6.92 and 6.89 ppm was attributed to the HC= proton adjacent to the thiazole ring, while another doublet at δ6.79 and 6.77 ppm was assigned to the O=C–CH proton α- to the carbonyl group. Finally, a singlet at δ3.52 ppm was attributed to the methyl (CH$_3$) group. The ^{1}H-NMR spectrum is shown in Fig. 2.

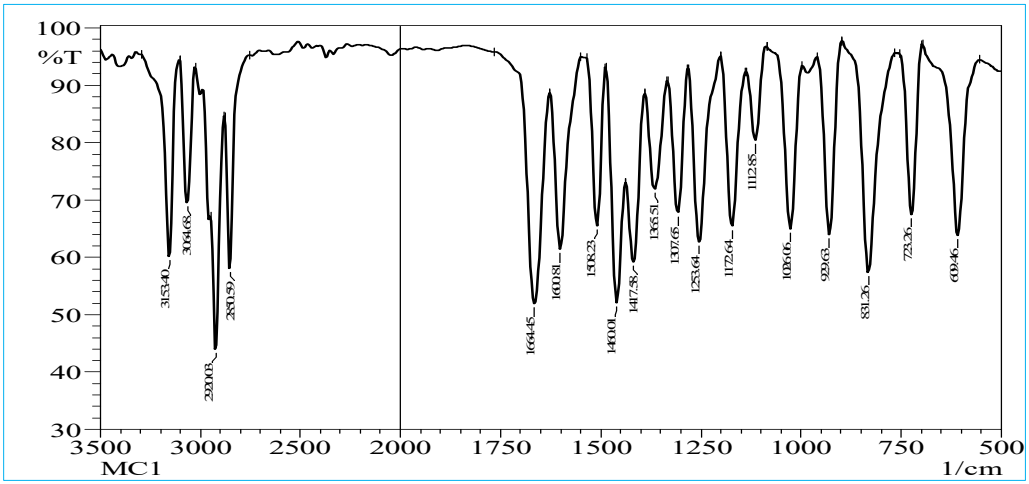

Fig. 1. FT-IR spectrum of the compound (MC$_1$)

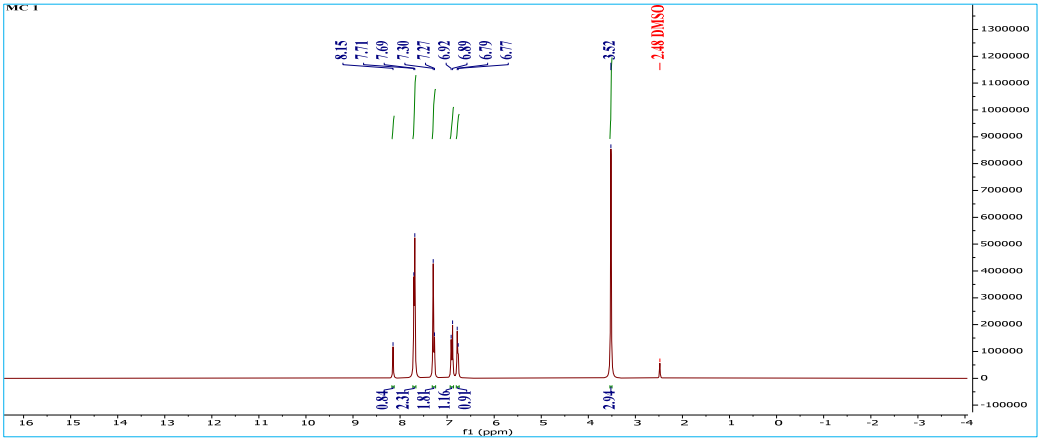

Fig. 2. ^{1}H-NMR spectrum of the compound (MC$_1$)

The ^{13}C-NMR spectrum of compound MC$_1$ was recorded in DMSO-d$_6$. A signal at δ189.00 ppm was assigned to the carbonyl carbon (C=O), while a signal at δ161.85 ppm corresponded to the C=N carbon in the thiazole ring. The carbon of the =CH group adjacent to the thiazole ring appeared at δ142.00 ppm, and the O=C–CH carbon α- to the carbonyl group was observed at δ121.09 ppm. Signals in the range δ123.09–150.47 ppm were attributed to aromatic ring carbons. The ^{13}C-NMR spectrum is shown in Fig. 3.

3.2. Characterization of 2-Oxo pyrimidine derivatives (MC$_6$-MC$_{10}$). The IR spectrum exhibited a new absorption band in the range 3278–3235 cm^{-1}, attributed to N–H stretching vibrations. The olefinic (C=C) absorption band of the chalcones (MC1–MC5), previously observed at 1616–1600 cm^{-1}, disappeared. Instead, a medium-intensity band corresponding to the carbonyl group (C=O) of the pyrimidine ring appeared in the range 1684–1677 cm^{-1}. An absorption band assigned to the C=N group was observed at 1627–1619 cm^{-1}. Additional bands at 1589–1547 cm^{-1} and 1485–1465 cm^{-1} corresponded to C=C stretching vibrations of the aromatic ring. Aliphatic C–H stretching vibrations were detected at 2954–2920 cm^{-1} and 2883–2843 cm^{-1}, while aromatic C–H (Ar–CH) stretching was observed at 3048–3068

cm^{-1} [19–21]. The spectral data are summarized in Table 3, and representative spectra are shown in Fig. 4.

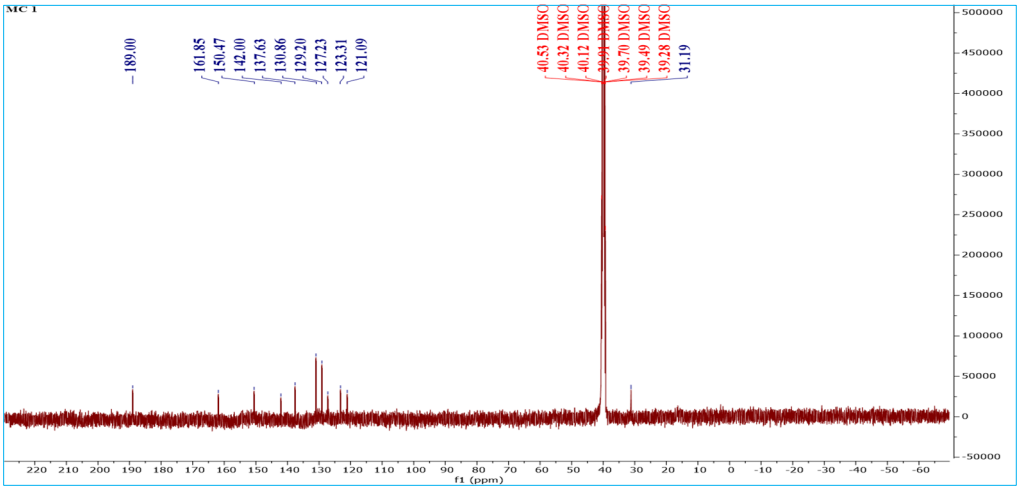

Fig. 3. ^{13}C-NMR spectrum of the compound (MC_1)

Table 3. FT-IR absorption results for 2-Oxo pyrimidine derivatives (MC_6-MC_{10})

Comp. No.	R	IR (KBr) cm^{-1}						
		ν(C-H) Arom.	ν(N-H)	ν(C-H) Aliph.	ν(C=N)	ν(C=O)	ν(C=C) Arom.	Others
MC_6	Br	3048	3235	2923 2865	1621	1684	1553 1471	ν (C-Br) 616
MC_7	NO_2	3068	3263	2920 2848	1622	1679	1589 1485	ν (NO_2) *asy*. (1541) *sym*. (1352)
MC_8	OCH_3	3054	3278	2921 2853	1621	1682	1547 1481	ν C-O-C Asy: 1332 sym: 1271
MC_9	H	3066	3247	2951 2843	1619	1677	1572 1465	---
MC_{10}	Cl	3058	3261	2954 2883	1627	1679	1583 1485	ν (C-Cl)746

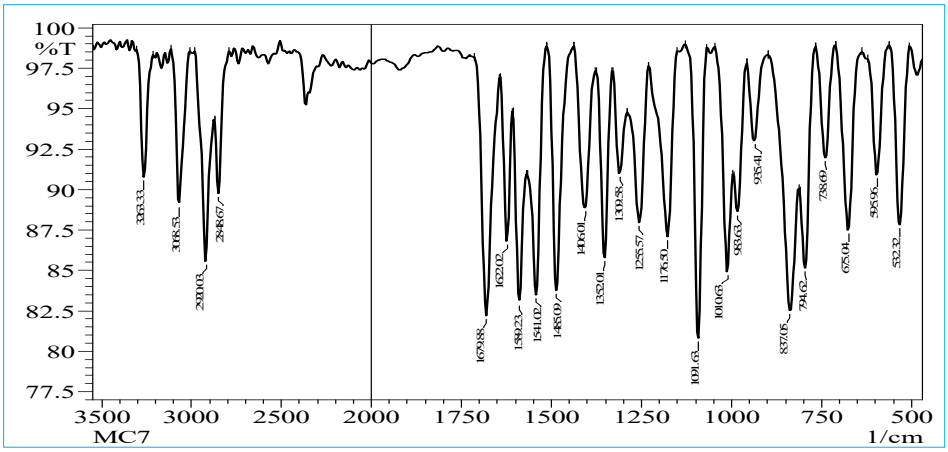

Fig. 4. FT-IR spectrum of the compound (MC_7)

The ^{1}H-NMR spectrum of compound (MC_7) (DMSO-d_6) showed a singlet at δ8.37 ppm, assigned to the (N=CH) proton of the thiazole ring. Multiplet signals in the range δ7.77–8.08 ppm corresponded to aromatic protons, while a singlet at δ7.00 ppm was attributed to the (NH) proton. A triplet at δ3.69–3.74 ppm was assigned to the aliphatic (CH)

proton, and a doublet at δ2.38 and 2.41 ppm was attributed to the two protons of the (CH_2) group. Finally, a singlet at δ1.99 ppm corresponded to the protons of the (CH_3) group. The spectrum is shown in Fig. 5.

The ^{13}C-NMR spectrum of compound (MC_7) (DMSO-d_6) showed a signal at δ166.98 ppm assigned to the (C=N) carbon of the pyrimidine ring, and a signal at δ164.46 ppm corresponding to the (C=O) carbon. The (C=N) carbon in the thiazole ring appeared at δ156.04 ppm. Signals for aromatic carbons were observed in the range δ 129.08–140.72 ppm. The (CH) carbon resonated at δ56.51 ppm, the (CH_2) carbon at δ51.74 ppm, and the (CH_3) carbon at δ15.99 ppm. The spectrum is presented in Fig. 6.

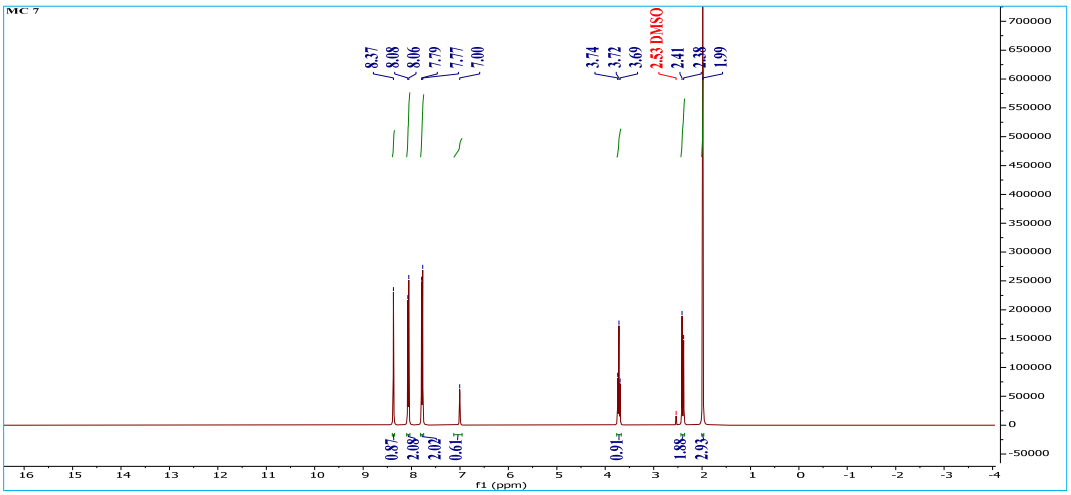

Fig. 5. ^{1}H-NMR spectrum of the compound (MC_7)

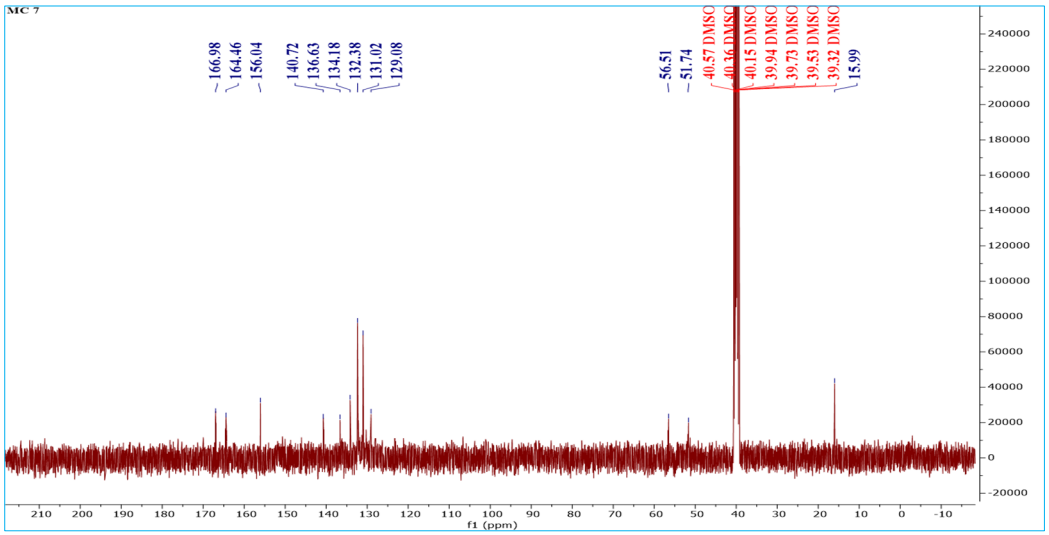

Fig. 6. ^{13}C-NMR spectrum of the compound (MC_7)

3.3. Characterization of 2-thio pyrimidine derivatives (MC_{11}-MC_{15}). The IR spectrum displayed an absorption band for the C=N group at 1630–1622 cm^{-1}, along with a new band at 3254–3210 cm^{-1} attributed to N–H stretching vibrations. The olefinic C=C band of the chalcones (MC_1–MC_5), previously observed at 1616–1600 cm^{-1}, was absent. A medium-intensity band in the range 1087–1097 cm^{-1} corresponded to the C=S group of the pyrimidine ring. Additional bands at 1581–1548 cm^{-1} and 1485–1460 cm^{-1} were assigned to C=C stretching vibrations of the aromatic ring.

Aliphatic C–H stretching bands appeared at 2981–2953 cm^{-1} and 2900–2842 cm^{-1}, while aromatic C–H (Ar–CH) stretching was observed at 3043–3070 cm^{-1}. The spectral data are summarized in Table 4, and representative spectra are shown in Fig. 7.

Table 4. FT-IR absorption results for 2-Thio pyrimidine derivatives (MC_{11}-MC_{15})

Comp. No.	R	IR (KBr) cm^{-1}						
		ν(C-H) Aliph.	ν(C-H) Arom.	ν(N-H)	ν(C=N)	ν(C=S)	ν(C=C) Arom.	Others
MC_{11}	Br	2981 2900	3062	3232	1629	1093	1556 1477	ν (C-Br) 624
MC_{12}	NO_2	2965 2842	3043	3254	1630	1097	1564 1465	ν(NO_2) *asy*. (1507) *sym*. (1338)
MC_{13}	OCH_3	2979 2891	3070	3210	1620	1087	1581 1485	νC-O-C Asy: 1332 sym: 1272
MC_{14}	H	2967 2859	3061	3243	1626	1089	1548 1467	---
MC_{15}	Cl	2953 2871	3051	3235	1622	1102	1567 1460	ν (C-Cl)753

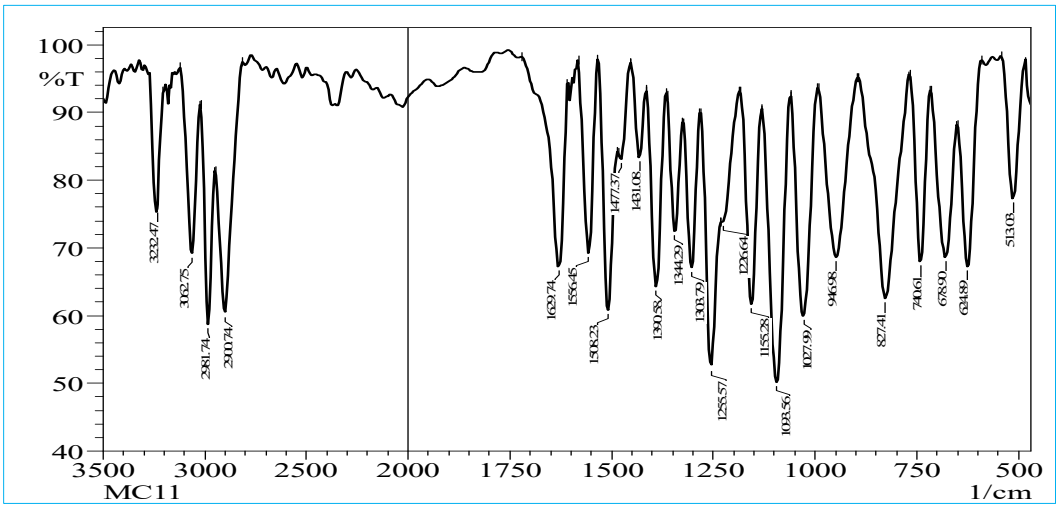

Fig. 7. FT-IR spectrum of the compound (MC_{11})

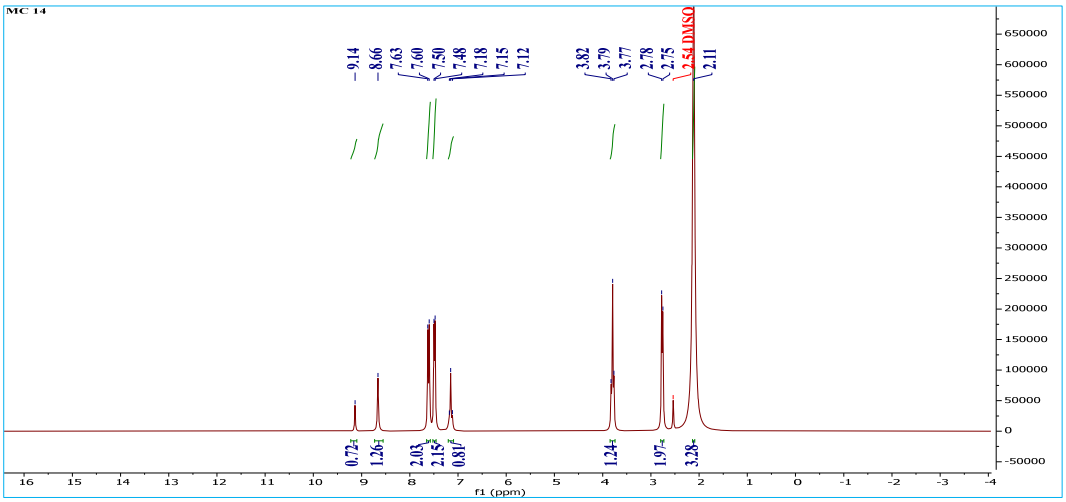

Fig. 8. ^{1}H-NMR spectrum of the compound (MC_{14})

^{1}H-NMR (DMSO-d_6). A singlet at δ 9.14 ppm was assigned to the NH proton, while the N=CH proton in the thiazole ring appeared as a singlet at δ 8.66 ppm. Multiple signals in the range δ 7.12–7.63 ppm corresponded to aromatic protons. A triplet at δ 3.77–3.82 ppm was attributed to the aliphatic CH proton, and a doublet at δ 2.75 and 2.78 ppm was assigned to

the two protons of the CH_2 group. A singlet at δ 2.11 ppm corresponded to the CH_3 protons (Fig. 8).

^{13}C-NMR (DMSO-d_6). A signal at δ 183.05 ppm was assigned to the C=S carbon, while the C=N carbons in the pyrimidine and thiazole rings appeared at δ 160.01 ppm and δ 155.58 ppm, respectively. Aromatic carbons resonated in the range δ 123.04–141.99 ppm. The CH carbon was observed at δ 52.57 ppm, the CH_2 carbon at δ 46.89 ppm, and the CH_3 carbon at δ 19.03 ppm (Fig. 9).

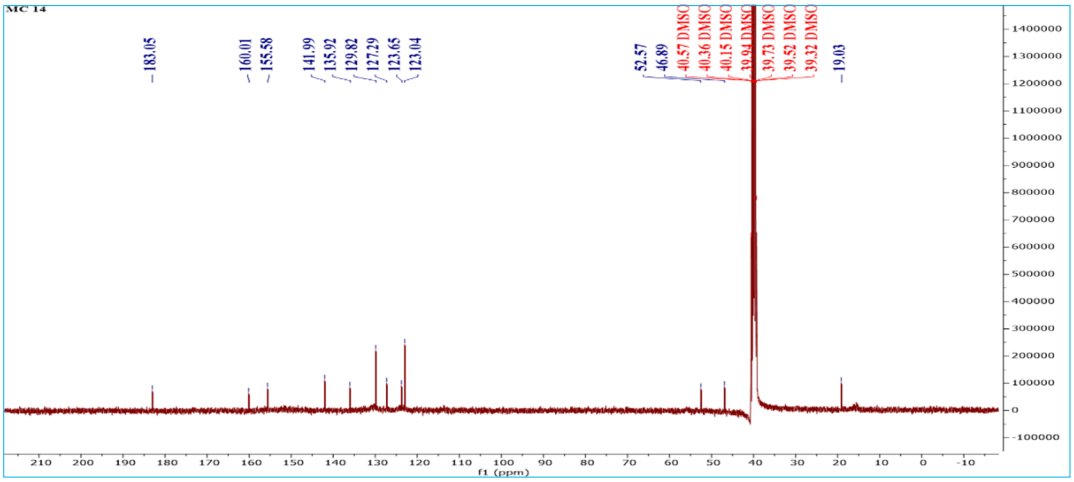

Fig. 9. ^{13}C-NMR spectrum of the compound (MC_{14})

3.4. Characterization of 2-cyanamide pyrimidine derivatives (MC_{16}-MC_{20}). The FT-IR spectra of compounds MC16–MC20 showed the disappearance of the olefinic (C=C) and carbonyl (C=O) bands characteristic of the chalcones. N–H stretching vibrations were observed in the range 3232–3359 cm^{-1}. Aromatic C–H (Ar–CH) stretching appeared at 3047–3080 cm^{-1}, while aliphatic C–H stretching bands were detected at 2920–2966 cm^{-1} and 2852–2891 cm^{-1}. Aromatic C=C stretching was observed at 1579–1565 cm^{-1} and 1484–1456 cm^{-1}. In addition, C≡N stretching vibrations appeared in the range 2090–2131 cm^{-1}. The spectral data are summarized in Table 5, and representative spectra are shown in Fig. 10.

Table 5. FT-IR absorption results for 2-cyanamide pyrimidine derivatives (MC_{16}-MC_{20})

Comp. No.	R	ν (C-H) Arom	IR (KBr) cm^{-1}						
			ν (NH)	ν (C-H) .Aliph.	ν (CN)	ν(C=N)	ν(C=C) Arom.	ν(C-N)	Others
MC_{16}	Br	3047	3258	2953 2862	2131	1628	1557 1456	1223	ν (C-Br) 672
MC_{17}	NO_2	3059	3232	2966 2891	2104	1620	1579 1481	1232	ν (NO_2) *asy*.(1510) *sym*. (1340)
MC_{18}	OCH_3	3080	3234	2920 2852	2096	1624	1566 1475	1188	ν C-O-C Asy: 1354 sym: 1305
MC_{19}	H	3069	3245	2940 2859	2090	1626	1565 1456	1195	---
MC_{20}	Cl	3075	3259	2937 2861	2105	1627	1578 1484	1203	ν (C-Cl)801

The ^{1}H-NMR spectrum of (MC_{18}) showed that the proton of the (N=CH) group in the thiazole ring was responsible for a single signal at position 8.49 ppm, the protons of the benzene ring were responsible for a multiple signal in the range 7.25-7.69 ppm, the proton of the aliphatic group (CH) was responsible for a triple signal in the range 3.96-4.02 ppm, the protons of the

(OCH_3) group were responsible for a single signal at position 3.52 ppm, a double signal appeared at positions 2.73 and 2.75 ppm, responsible for the (CH_2) proton, the protons of the (CH_3) group were responsible for a single signal at position 2.35 ppm, and the proton of the (NH) group was responsible for a signal at position 1.19 ppm, as shown in Fig. 11.

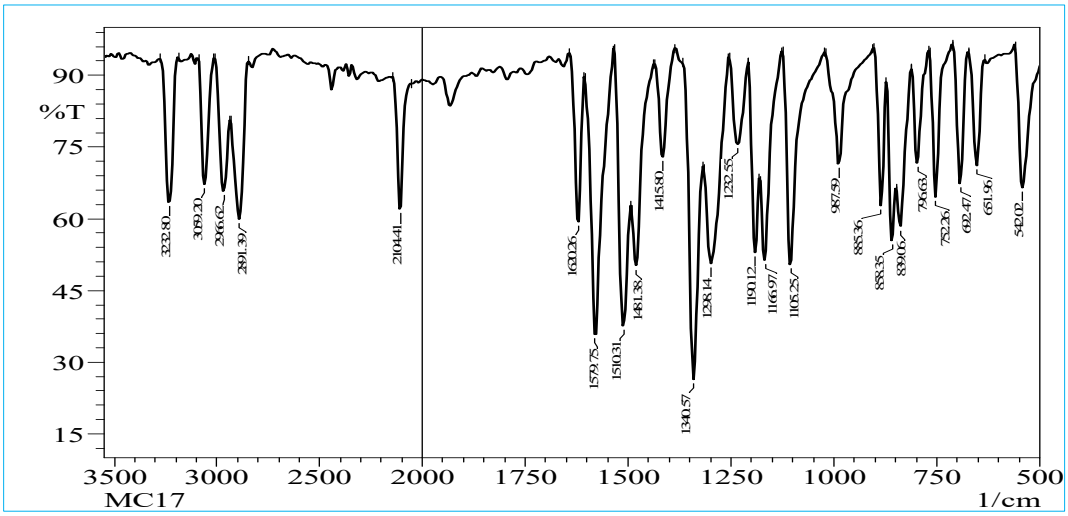

Fig. 10. FT-IR spectrum of the compound (MC_{17})

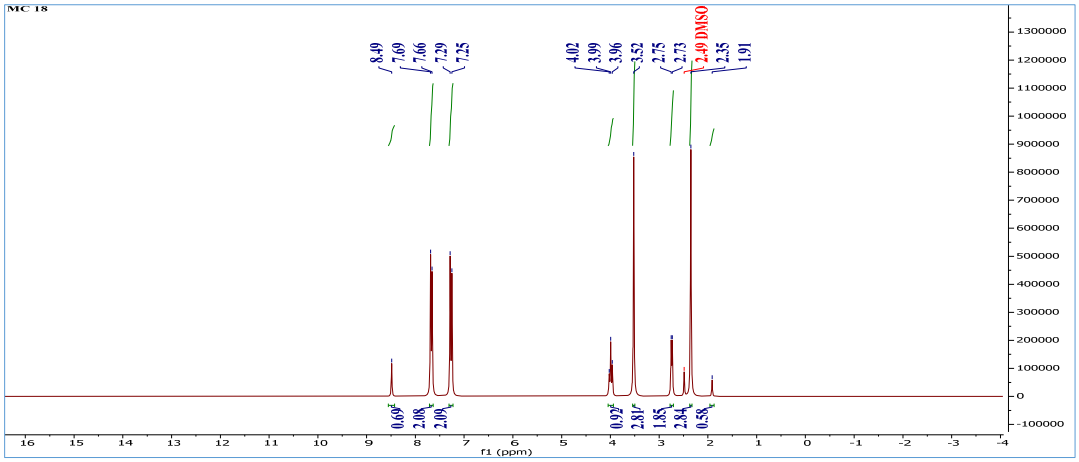

Fig. 11. ^{1}H-NMR spectrum of the compound (MC_{18})

When examining the compound (MC_{18}) ^{13}C-NMR spectrum, a signal was detected at position 169.97 ppm that was attributed to the carbon of the (C=N) group in the pyrimidine ring, at position 152.02 ppm that was attributed to the carbon of the (C=N) group next to the (CN) group, at position 149.97 ppm that was attributed to the carbon of the (C=N) group in the thiazole ring, and at positions 129.19-158.37 ppm that were attributed to the carbons of the aromatic benzene ring, at position 124.63 that was attributed to the carbon of the (CN) group, at position 60.88 ppm that was attributed to the carbon of the (OCH_3) group. Additionally, the presence of a signal at site 52.28 ppm was caused by the carbon of the aliphatic (CH) group, at site 36.37 ppm by the carbon of the (CH_2) group, and at site 31.19 ppm by the carbon of the (CH_3) group. As shown in Fig. 12.

3.5. Evaluation of the Biological Activity of Prepared Compounds. The selected bacterial strains are medically significant due to their association with a wide range of infections and their varying degrees of drug resistance. The antibacterial activity of some synthesized compounds was evaluated using the agar well diffusion method, with inhibition zone diameters measured to assess efficacy. The results indicate that the compounds exhibit varying degrees of inhibitory effects against both Gram-positive and Gram-negative bacteria [22–25].

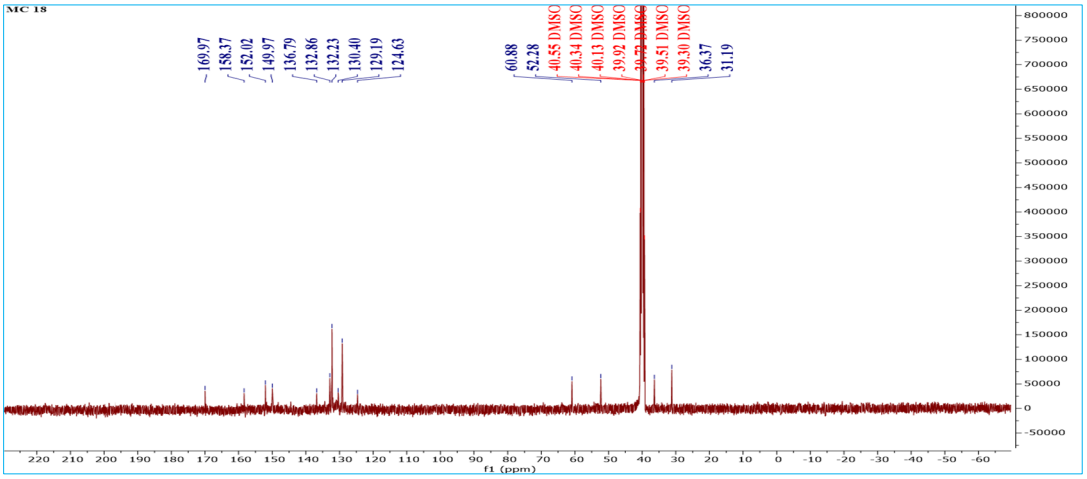

Fig. 12. ^{13}C-NMR spectrum of the compound (MC_{18})

Table 6. Biological effectiveness of prepared compounds and control treatments (inhibition in mm)

Comp. No.	***Escherichia coil***			***Staphylococcus aureus***		
Conc. mg/ml	0.1	0.01	0.001	0.1	0.01	0.001
MC_1	**25**	25	**30**	18	15	10
MC_4	**24**	23	**20**	22	17	12
MC_5	**23**	20	**18**	20	15	15
MC_7	**18**	16	**12**	19	18	13
MC_8	**18**	18	**9**	20	18	10
MC_{10}	**30**	20	**18**	17	15	10
MC_{13}	**35**	27	**12**	30	20	15
MC_{14}	**32**	26	**21**	24	18	13
MC_{15}	**20**	20	**18**	27	18	12
MC_{16}	**16**	15	**9**	32	23	15
MC_{20}	**18**	18	**15**	15	12	10
Amoxicillin	24	16	10	20	10	10
Ciprofloxacin	20	15	15	15	12	12
Amikasin	15	15	10	10	10	8

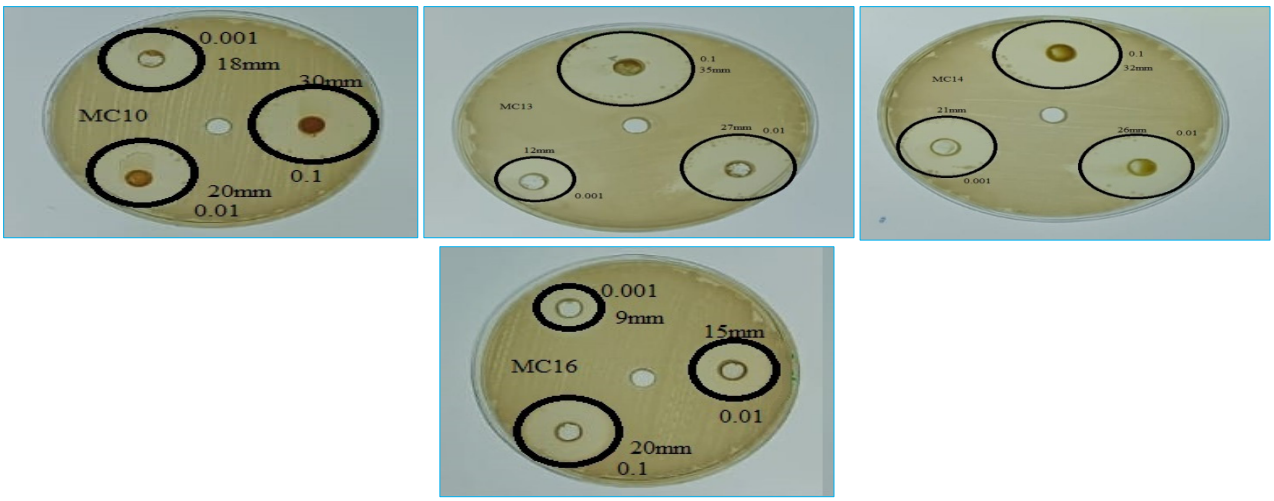

Fig. 13. Inhibitory activity of compounds (MC_{10}, MC_{13}, MC_{14}, MC_{16}) against *Escherichia coli*

Standard antibiotics—amoxicillin, amikacin, and ciprofloxacin—were used as control samples due to their well-established selectivity and broad inhibitory zones [26–30]. Among the tested compounds, MC13 showed the highest inhibitory activity against *Escherichia coli*, with a zone of inhibition measuring 35 mm. Compounds (MC_{10} and MC_{14}) also exhibited significant activity against *E. coli*, with inhibition zones of 32 mm and 30 mm, respectively. Against *Staphylococcus aureus*, (MC_{16}) demonstrated the greatest inhibitory effect (32 mm), while MC13 showed good activity with a 30 mm inhibition zone.

Other compounds showed moderate to good antibacterial activity. A direct relationship was observed between compound concentration and inhibition efficacy, with the highest inhibition zones recorded at 0.1 mg/mL [31, 32]. Detailed results are presented in Table 7 and Fig.s 13 and 14.

Fig. 14. Inhibitory activity of compounds (MC_4, MC_8, MC_{13}, MC_{15}) against *Staphylococcus aureus*

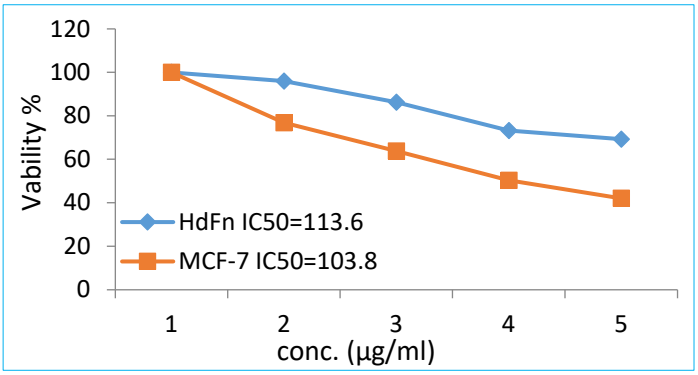

Fig. 15. The effect of the compound (MC_7) on MCF-7 cells and HdFn cells using the MTT assay

3.7. Results of the breast cancer cytotoxicity test study (MCF-7). This study evaluated the effect of the compounds (MC_7, MC_{15}, and MC_{19}) on normal HdFn cells and MCF-7 breast cancer cells at different concentrations (50, 100, 200, and 400 µg/ml). The results demonstrated a dose-dependent cellular response, with cancer cell survival decreasing with increasing concentration ($P \leq 0.0001$), while normal cells were less affected, suggesting the compounds may possess selectivity against cancer cells [33-35].

For compound (MC_7), the average survival of MCF-7 cells at 400 µg/ml was 42.05%, demonstrating a strong effect at high concentrations. Furthermore, as the concentration decreased, the average survival gradually increased, but the effect remained greater on cancer cells compared to normal cells, indicating a degree of selectivity, as shown in Fig. s (15, 16).

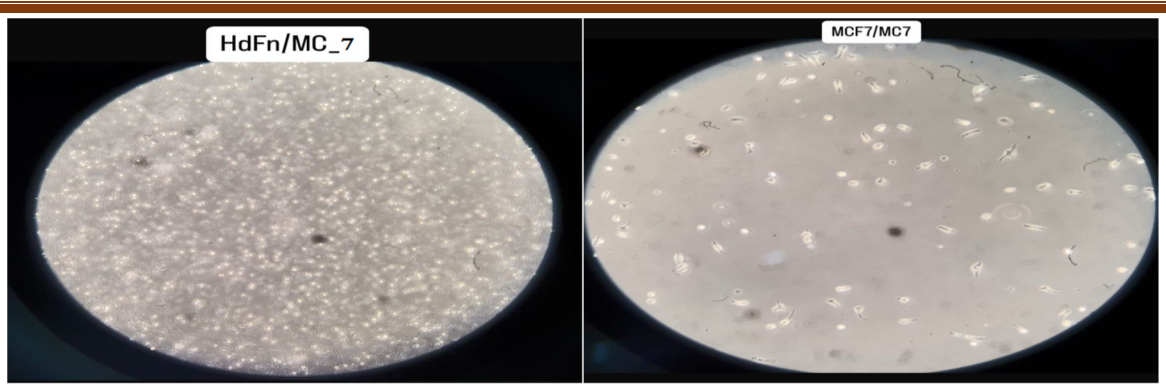

Fig. 16. The effectiveness of the compound (MC_7) on MCF-7 cells and HdFn cells

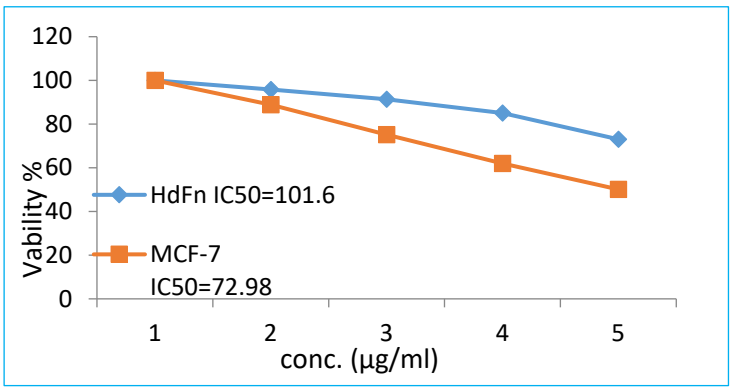

Fig. 17. The effect of the compound (MC_{15}) on MCF-7 cells and HdFn cells using the MTT assay

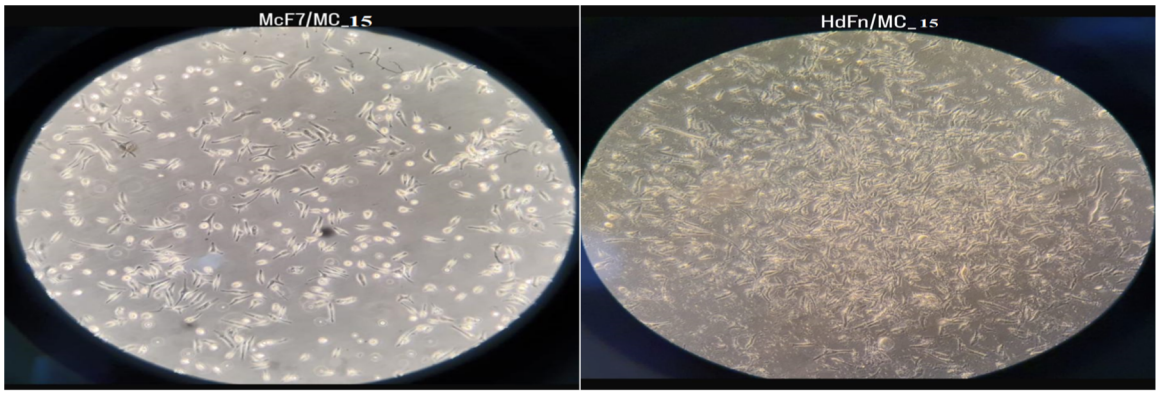

Fig. 18. The effectiveness of the compound (MC_{15}) on MCF-7 cells and HdFn cells

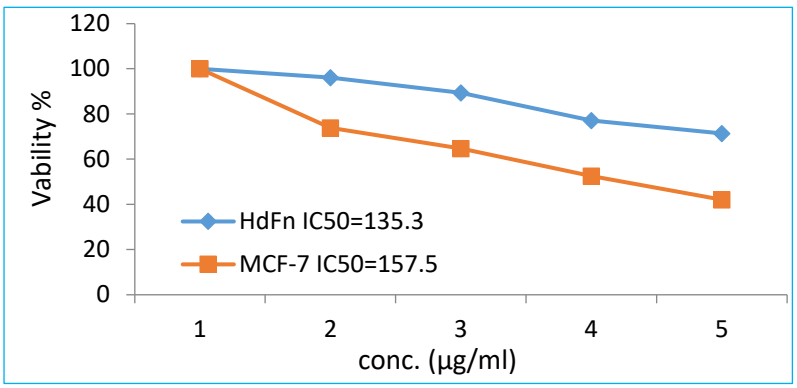

Fig. 19. The effect of the compound (MC_{19}) on MCF-7 cells and HdFn cells using the MTT assay

MC_{15} had a clear effect on MCF-7 cells, recording a 50.11% survival rate at a concentration of 400 µg/ml compared to 73.03% for HdFn cells, indicating a greater decrease in

cancer cell viability at higher concentrations. As the concentration was reduced, the mean survival rate gradually increased, reflecting a dose-dependent response, as shown in Fig. s 17 and 18.

MC_{19} appeared to be more effective against MCF-7 cells, recording a 42.05% survival rate at a concentration of 400 µg/ml, which is lower than the rate recorded for MC_{15} at the same concentration, potentially indicating a stronger effect. When the concentration was reduced to 50 µg/ml, the survival rate increased to 76.81% in MCF-7 cells. At the same time, it remained high in HdFn cells, with a survival rate of 95.98%, indicating a reduced toxic effect on normal cells at lower doses (Fig. s 19 and 20).

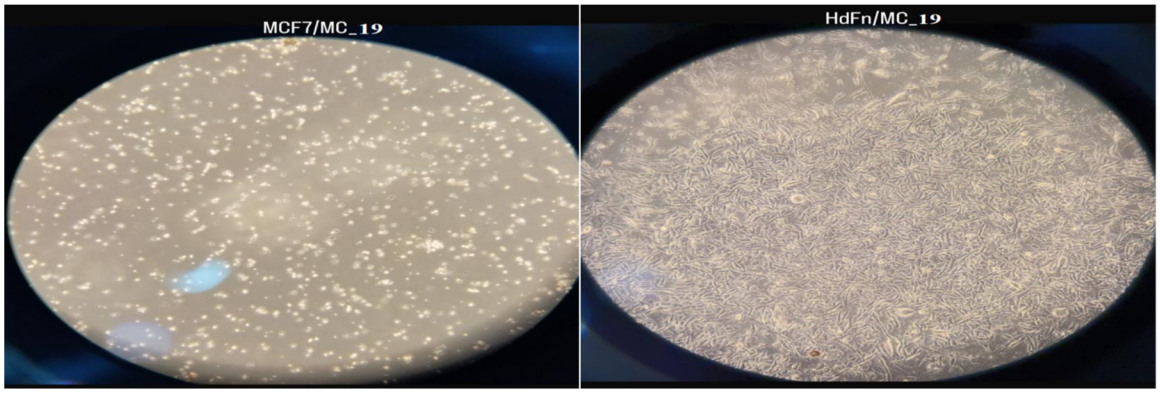

Fig. 20. The effectiveness of the compound (MC_{19}) on MCF-7 cells and HdFn cells

The results indicate that the two compounds (MC_{19} and MC_7) showed a stronger effect on cancer cells than (MC_{15}), especially at high concentrations. All compounds also possessed a certain degree of selectivity, affecting MCF-7 cells to a greater extent than HdFn cells, making them candidates for further studies in the development of anticancer drugs.

4. Conclusions

Hexagonal pyrimidine rings were synthesized via the reaction of α,β-unsaturated compounds with reagents containing various functional groups. Spectroscopic analyses confirmed the structural accuracy and purity of the synthesized compounds. Biological evaluation revealed that most of these compounds exhibit significant antibacterial activity, effectively inhibiting bacterial growth. Notably, some compounds demonstrated superior activity compared to the standard antibiotics used as controls. Specifically, compound (MC_{13}) showed the highest inhibitory effect against *Escherichia coli*, with an inhibition zone of 35 mm, while compound (MC_{16}) was most effective against *Staphylococcus aureus*, exhibiting an inhibition zone of 32 mm. Additionally, several compounds showed promising cytotoxic activity against cancer cells, warranting further investigation to develop potential therapeutic agents for cancer treatment.

References

1. Sung H., Ferlay J., Siegel R.L., Laversanne M., Soerjomataram I., Jemal A., Bray F. Global cancer statistics 2020: GLOBOCAN estimates of incidence and mortality worldwide for 36 cancers in 185 countries. *CA: a cancer journal for clinicians*, 2021, **Vol. 71(3)**, p. 209-249. DOI: 10.3322/caac.21660
2. Heravi M.M., Zadsirjan V. Prescribed drugs containing nitrogen heterocycles: an overview. *RSC advances*, 2020, **Vol**. 10(72), p. 44247-44311. DOI: 10.1039/D0RA09198G
3. Martins P., Jesus J., Santos S., Raposo L.R., Roma-Rodrigues C., Baptista P.V., Fernandes A.R. Heterocyclic anticancer compounds: recent advances and the paradigm shift towards the use of nanomedicine's tool box. *Molecules*, 2015, **Vol**. **20(9),** p. 16852-16891. DOI: 10.3390/molecules200916852

4. Ajani O.O., Audu O.Y., Aderohunmu D.V., Owolabi F.E., Olomieja A.O. Undeniable pharmacological potentials of quinazoline motifs in therapeutic medicine. *Am. J. Drug Discov. Dev.* 2017, **Vol**. **7(1)**, p. 1-24. DOI: 10.3923/ajdd.2017.1.24
5. Özkay Y., Işıkdağ İ., İncesu Z., Akalın G. Synthesis of 2-substituted-N-[4-(1-methyl-4, 5-diphenyl-1H-imidazole-2-yl) phenyl] acetamide derivatives and evaluation of their anticancer activity. *European journal of medicinal chemistry*, 2010, **Vol**. **45(8)**, p. 3320-3328. DOI: 10.1016/j.ejmech.2010.04.015
6. Chiacchio M.A., Iannazzo D., Romeo R., Giofrè S.V., Legnani L. Pyridine and pyrimidine derivatives as privileged scaffolds in biologically active agents. *Current medicinal chemistry*, 2019, **Vol**. **26(40)**, p. 7166-7195. DOI: 10.2174/0929867325666180904125400
7. Prachayasittikul S., Pingaew R., Worachartcheewan A., Sinthupoom N., Prachayasittikul V., Ruchirawat S., Prachayasittikul V. Roles of pyridine and pyrimidine derivatives as privileged scaffolds in anticancer agents. *Mini Reviews in Medicinal Chemistry*, 2017, **Vol. 17(10)**, p. 869-901. DOI: 10.2174/1389557516666160923125801
8. Al-Joboury N.A., Al-Badrany K.A., Hamed A.S., Aljoboury W.M. Synthesis of some new thiazepine compounds derived from chalcones and evaluation there biochemical and biological activity. *Biochemical & Cellular Archives*, 2019, **Vol. 19(2),** p. 4545-4554. DOI: 10.35124/bca.2019.19.2.4545
9. Al-Tufah M.M., Jasim S.S., Al-Badrany K.A. Synthesis and Antibacterial Evaluation of some New Pyrazole Derivatives. *Prof.(Dr) RK Sharma*, 2020, **Vol**. **20(3)**, 178.
10. Tolba M.S., El-Dean A., Ahmed M., Hassanien R., Sayed M., Zaki R., Mohamed Sh.K., Zawam S.A., Abdel-Raheem S. Synthesis, reactions, and applications of pyrimidine derivatives. *Current Chemistry Letters*, 2022, **Vol**. **11**, p. 121-138. DOI: 10.5267/j.ccl.2021.008.002
11. Kumar A., Kumar P. Green chemistry approaches in the synthesis of pyrimidine derivatives. *Rasayan Journal of Chemistry*, 2023, **Vol. 16(3)**, p. 1844-1848. DOI: 10.31788/RJC.2023.1638357
12. Abdullah S.H., Salih M.M., Al-Badrany A. Synthesis, Characterization and Antibacterial Evaluation of Novel Thiazolidine Derivatives. *Journal of Angiotherapy*, 2024, **Vol**. **8(3)**, p. 1-9. DOI: 10.25163/angiotherapy.839501
13. Aftan M.M., Talloh A.A., Dalaf A.H., Salih H.K. Impact para position on rho value and rate constant and study of liquid crystalline behavior of azo compounds. *Materials Today: Proceedings*, 2021, **Vol**. 45(6), p. 5529-5534. DOI: 10.1016/j.matpr.2021.02.298
14. Al-Joboury W.M., Al-Badrany K.A., Asli N.J. N-alkylation of substituted 2-amino benzothiazoles by 1, 4-bis (bromo methyl) benzene on mixed oxides at room temperature and study their biological activity. In *AIP Conference Proceedings*. 2022, **Vol. 2394**, 040054. DOI: 10.1063/5.0123463
15. Badawi W.A., Samir M., Fathy H.M., Okda T.M., Noureldin M.H., Atwa G.M., AboulWafa O.M. Design, synthesis and molecular docking study of new pyrimidine-based hydrazones with selective anti-proliferative activity against MCF-7 and MDA-MB-231 human breast cancer cell lines. *Bioorganic Chemistry*, 2023, **Vol**. **138**, 106610. DOI: 10.1016/j.bioorg.2023.106610
16. Shi D., Xu W., Wong M., Popovich D.G. An improved purification method for removing colour interference from 3-(4, 5-dimethylthiazol-2-yl)-2, 5-diphenyl tetrazolium bromide (MTT) antibacterial assays. *Applied Sciences*, 2023, **Vol**. **13(8)**, 5067. DOI: 10.3390/app13085067
17. Wilhelm A., Bonnet S.L., Twigge L., Rarova L., Stenclova T., Visser H.G., Schutte-Smith M. Synthesis, characterization and cytotoxic evaluation of chalcone derivatives. *Journal of Molecular Structure*, 2022, **Vol. 1251**, 132001. DOI: 10.1016/j.molstruc.2021.132001
18. Bandeira N.P., Lemos T.L.G., Santos S.H., de Carvalho M.C.S., Pinheiro D.P., de Moraes Filho M.O., Pessoa C., Barros-Nepomuceno F.W.A., Rodrigues T.H.S., Ribeiro P.R.V., Magalhães H.S., Teixeira

A.M.R. Synthesis, structural characterization, and cytotoxic evaluation of chalcone derivatives. *Medicinal Chemistry Research*, 2019, **Vol**. **28**, p. 2037-2049. DOI: 10.1007/s00044-019-02434-1
19. Heakal F.E.T., Rizk S.A., Elkholy A.E. Characterization of newly synthesized pyrimidine derivatives for corrosion inhibition as inferred from computational chemical analysis. *Journal of Molecular Structure*, 2018, **Vol**. **1152**, p. 328-336. DOI: 10.1016/j.molstruc.2017.09.079
20. Masoud M.S., Sweyllam A.M., Ahmed M.M. Synthesis, characterization, coordination chemistry and biological activity of some pyrimidine complexes. *Journal of Molecular Structure*, 2020, **Vol. 1219**, 128612. DOI: 10.1016/j.molstruc.2020.128612
21. Zhuo L., Kou K., Wang Y., Chen H. Synthesis and characterization of pyrimidine-containing hyperbranched polyimides. *Designed Monomers and Polymers*, 2015, **Vol**. **18(1)**, p. 42-50. DOI: 10.1080/15685551.2014.947552
22. Alrashidy A.A.M., Hashem O.A., ALBadrany K.A.A. Spectrophotometric Determination of Vitamin C Using Indirect Oxidation with a New Organic Dye. *Journal of Angiotherapy*, 2024, **Vol. (2)**, p. 1-7. DOI: 10.25163/angiotherapy.829499
23. Muhammad F.M., Khairallah B.A., Albadrany K.A. Synthesis, characterization and antibacterial evaluation of novel 1, 3-oxazepine derivatives using a cycloaddition approach. *Journal of Angiotherapy*, 2024, **Vol**. **(3)**, p. 1-5. DOI: 10.25163/angiotherapy.839506
24. Shannak Q.A., Mawlood M.K., Hebeb H.R. Characteristic studying and biological effect of synthesized complexes Pd (II) and Hg (II) with uracil dithiocarbamate and phosphine's. *Systematic Reviews in Pharmacy*, 2020, **Vol. 11(3)**, p. 693-701. DOI: 10.31838/srp.2020.3.94
25. Najm R.S., Shannak Q.A., Azeez A.S., Altekrity S., Al-Bayati H.H. Chemical Characteristic and Biological Activity of Silver Nanoparticles on *Sidr* Leaves (*Zizyphus Spina-Christi*) Extract. *Advanced Journal of Chemistry, Section A*, 2025, **Vol**. **8(10)**, p. 1640-1650. DOI: 10.48309/ajca.2025.511360.1802
26. Khadm N.J., Shannak Q.A., Ibraheem T.K. Synthesis new derivatives of Azo compounds contain a Schiff bases and evaluate their biological activity. *Edelweiss Applied Science and Technology*, 2024, **Vol**. **8(6)**, p. 9605-9608. DOI: 10.55214/25768484.v8i6.4061
27. Najm R.S., Shannak Q.A., Dalaf A.H. Synthesis and Decoration of Aromatic Derivatives Nano Platelets by the Electric Method. *Azerbaijan Pharmaceutical and Pharmacotherapy Journal*, 2023, **Vol. 22(2)**, p. 92-97. DOI: 10.61336/appj/22-2-22.
28. Al-Badrani H., Ezzat N.S., Al-Jawaheri Y.S. Synthesis of oxazepino compound via electrophilic cyclization and evaluation of their biological activity. *Chemical Problems*, 2025, **Vol. 23(3),** p. 343-355. DOI: 10.32737/2221-8688-2025-3-343-355
29. Murad Z.A., Hamad A.S. Preparation and diagnosis of new derivatives of the tetrazole ring derived from 2-bromoisophthaladehyde and evaluation of their biological effectiveness. *Chemical Problems*, 2025, **Vol. 23(1)**, p. 116-124. DOI: 10.32737/2221-8688-2025-1-116-124
30. Salih B.D., Mohammed A.S., Najm R.S., Mahmood A.R., Alheety M.A. Ortho-and Para-Nitrile Substituted Effect of (1H-Indol-2-Yl) Benzonitrile-Boehmite on the Nano Structures, Surface Area and Hydrogen Storage. *Energy Storage*, 2024, **Vol. 6**, e70034. DOI: 10.1002/est2.70034
31. Khalil S.L., Saleem N.H. Synthesis and characterization of five-membered heterocyclic compounds of tetrazole derivatives and their biological activity. *Chemical Problems*, 2025, **Vol**. **23(3)**, p. 365-374. DOI: 10.32737/2221-8688-2025-3-365-374
32. Hassan B.A., Mekky A.H. Synthesis, characterization and antibacterial activity of [1, 2, 4] triazolo [4, 3-b][1, 2, 4, 5] tetrazine derivatives. *Chemical Problems*, 2025, **Vol**. **23(1)**, p. 78-94. DOI: 10.32737/2221-8688-2025-1-78-94
33. Strubl S., Schubert U., Kühnle A., Rebl A., Ahmadvand N., Fischer S., Preissner K.T., Galuska S.P. Polysialic acid is released by human umbilical vein endothelial cells (HUVEC) in vitro. *Cell & bioscience*, 2018,

Vol. **64(8)**, p. 1-9. DOI: 10.1186/s13578-018-0262-y

34. Verma S., Prabhakar Y.S. Target based drug design-a reality in virtual sphere. *Current medicinal chemistry*, 2015, **Vol**. **(13),** p. 1603-1630. DOI: 10.2174/092986732266615020915120 9

35. Alasadi Y.K., Jumaa F.H., Dalaf A.H., Shawkat S.M., Mukhlif M.G. Synthesis, Characterization, and Molecular Docking of New Tetrazole Derivatives as Promising Anticancer Agents. *Journal of Pharmaceutical Negative Results*, 2022, **Vol**. **13(3)**, p. 513-522. DOI: 10.47750/pnr.2022.13.03.079